OPTIMIZATION OF A NOVEL SOLID-STATE SELF POWERED NEUTRON DETECTOR

Justin Dingley[a], Yaron Danon[a], Nicholas LiCausi[b], Jian-Qiang Lu[b] and Ishwara B. Bhat[b]
[a]Department of Mechanical, Aerospace and Nuclear Engineering,
[b]Department of Electrical, Computer and Systems Engineering,

Rensselaer Polytechnic Institute
110 8th St
Troy, NY 12180
dinglj@rpi.edu

ABSTRACT

Analytical and Monte Carlo calculations were performed to optimize a novel self-powered solid-state neutron detector. New manufacturing techniques, allowing for micron and sub-micron structures, along with the ability to efficiently collect the electron-hole pairs created in the detector, have resulted in improved theoretical thermal neutron detection efficiencies. Four differing configurations were examined, including a parallel-trench design, a pillar-type design, and two etched hole-type designs (square and hexagonal). First order analytical calculations provided initial parameter values for Monte Carlo simulations. Simulation results show the following maximum efficiencies: 40 percent efficiency for the pillar-type device, 43 percent for the parallel trench, 47 percent for the square hole device, and 48 percent for the hexagonal hole design.

Key Words: neutron, detection, optimization, solid-state

1. INTRODUCTION

Solid-state devices have been investigated for neutron detection numerous times over the years [1-6]. Although the specific configurations have changed, such as using several thin reactive films for thermal neutron detection, the inclusion of a hydrogenous material to detect fast neutrons via recoiled protons, or a combination of these two, all of these designs have suffered from extremely low (3-5%) detection efficiencies. Attempts to improve efficiency, including the utilization of a sandwich configuration, via-holes, and parallel trench designs, have met with limited success [7]. New manufacturing techniques [8] have enabled the creation of micron and sub-micron structures in silicon, with continuous, fully depleted solar-cell type p-n junctions throughout these structures. This results in increased electron-hole pair collection, allowing for the fabrication of higher efficiency detectors then were previously possible. To take full advantage of these advances, such a detector requires identification of parameters affecting efficiency and the optimization of these parameters. In this work it was decided to focus on the detection of thermal neutrons. As neutrons themselves would not interact appreciably with the silicon, a conversion material is required; absorption of the low energy neutrons produces charged particles, which can subsequently be detected. [10]B was chosen as the conversion material due to an extremely high thermal absorption cross section (3980 barns). Four basic designs were chosen for optimization: a parallel-trench design, in which trenches are etched into the silicon and filled with a neutron converter, a pillar type design, where most of the silicon has been etched away leaving pillars that are then surrounded by the converter, and square or hexagonal holes that have been etched and filled with converter. First order analytical calculations provided initial parameters for the Monte Carlo

simulations, which were then used to compare the designs and determine the optimal configuration.

2. METHODS

2.1. Analytical Calculations

There are three main factors influencing device efficiency; neutron interaction probability in the converter, the geometry of the device, and the ability of the charged particles resulting from neutron interaction in the absorption layer to escape into the silicon.

2.1.1. Neutron Interaction Probability

Consider a neutron beam incident normal to the surface of a planar converter; the probability of neutron interaction within the converter is

$$P(x) = 1 - e^{-\Sigma_t \cdot x_D} \tag{1}$$

where Σ_t is the total energy dependent macroscopic cross-section of the converter material, N is the number density of the material, and x_D converter depth. As stated previously, ^{10}B was used as the neutron converter for all the designs in this work. By assuming the incident neutrons are thermal (E = 0.0253 eV), and neglecting the small scattering cross-section, the total cross-section in equation 1 is replaced with the ^{10}B absorption cross-section Σ_a. By doing this, the interaction probability is simply a function of the converter depth x_D.

2.1.2. Device Geometry

The device geometry in the detector also affects detection efficiency. In the case neutrons incident normal to the surface of a planar detector, if the structures (holes, trenches, etc.) etched into the detector are also normal to the surface, the converter surface area fraction is proportional to the absorbed neutron fraction. Using a unit cell approach shown in figure 1, this geometric factor F can be calculated by
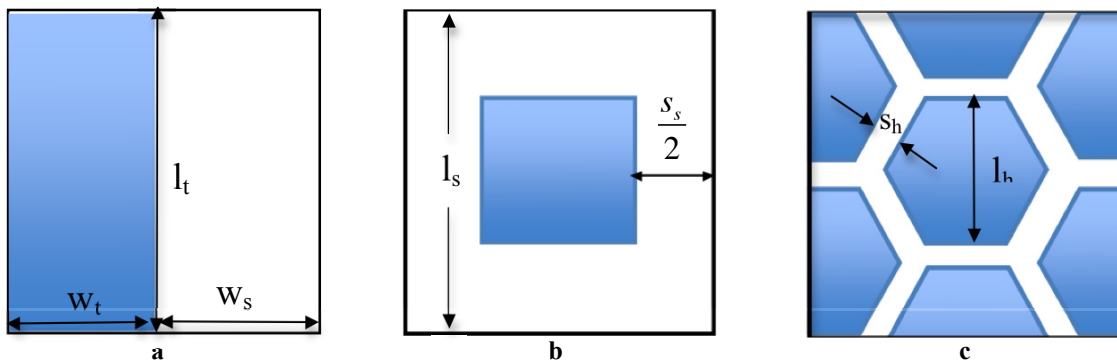

Figure 1: Unit cell configuration for trench (a), square hole (b), pillar (b), and hex hole (c) geometries.

2009 International Conference on Mathematics, Computational
Methods & Reactor Physics (M&C 2009), Saratoga Springs, NY, 2009

2/12

$$F_{trench} = \frac{l_t \cdot w_t}{(w_t + w_s) \cdot l_t} = \frac{w_t}{w_t + w_s} \tag{2}$$

for the trench design, where l_t is the device side length, w_t is the trench width, and w_s is the trench separation width. Equations 3 and 4 show the area fractions for the square hole and pillar designs, respectively, where l_s is the side length for the hole or the pillar and s_s is the separation between them. The factor for the hex hole is shown in equation 5, where l_h is the hexagon minor radius and s_h is the spacing between adjacent hexes.
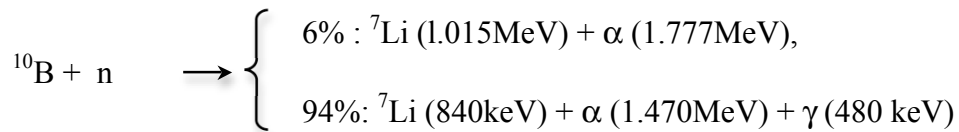
$$F_{square} = \frac{l_s^2}{(l_s + s_s)^2} \tag{3}$$

$$F_{pillar} = \frac{(l_s + s_s)^2 - l_s^2}{(l_s + s_s)^2} \tag{4}$$

$$F_{hex} = \frac{4 \cdot (\sqrt{3} \cdot l_h^2)}{\sqrt{3}(l_h + s_h)(2l_h + s_h)} \tag{5}$$

2.1.3. Charged Particle Detection

The last factor affecting detector efficiency is the ability of the charged particles resulting from neutron interaction in the absorption layer to escape into the silicon. The particles must have a minimum energy upon reaching the silicon to allow for adequate electron-hole pair collection. The continuous p-n junctions mentioned previously greatly improve electron-hole pair collection, allowing for a reduction in the low level detection (LLD) of 300 keV used in previous work [7]. For the work presented here, the LLD has been set to 200 keV per neutron. When a neutron is absorbed by ^{10}B, the following reactions occur

$$^{10}B + n \longrightarrow \begin{cases} 6\% : {}^{7}Li\,(1.015MeV) + \alpha\,(1.777MeV), \\ \\ 94\%: {}^{7}Li\,(840keV) + \alpha\,(1.470MeV) + \gamma\,(480\ keV) \end{cases}$$

Using the energies from the dominant reaction shown above, while ensuring that the minimum energy required for detection is retained, the particles have maximum ranges of 2.9 μm and 1.48 μm in ^{10}B for the alpha and lithium ion, respectively. Given its higher energy and greater range, the alpha particle will effect device efficiency to a greater extent than the lithium ion. As such, the analytical calculations were done solely for the alpha particle. Additionally, due to its large comparative range, the gamma photon is unlikely to deposit a significant amount of energy locally and therefore not included in the calculations.

The particle ranges can then be used to calculate the acceptance solid angle using

$$\Omega = \int\limits_{0}^{\phi} d\phi \int\limits_{\theta_1}^{\theta_2} \sin(\theta) \ d\theta \tag{6}$$

where ϕ is the azimuthal angle and θ is the polar angle. By assuming that neutron interaction is equally probable throughout the converter, and that particle emission in the converter is isotropic, the angles can be calculated using the particle range R and the distance L from the center of the converter to the closest silicon wall (fig. 2).
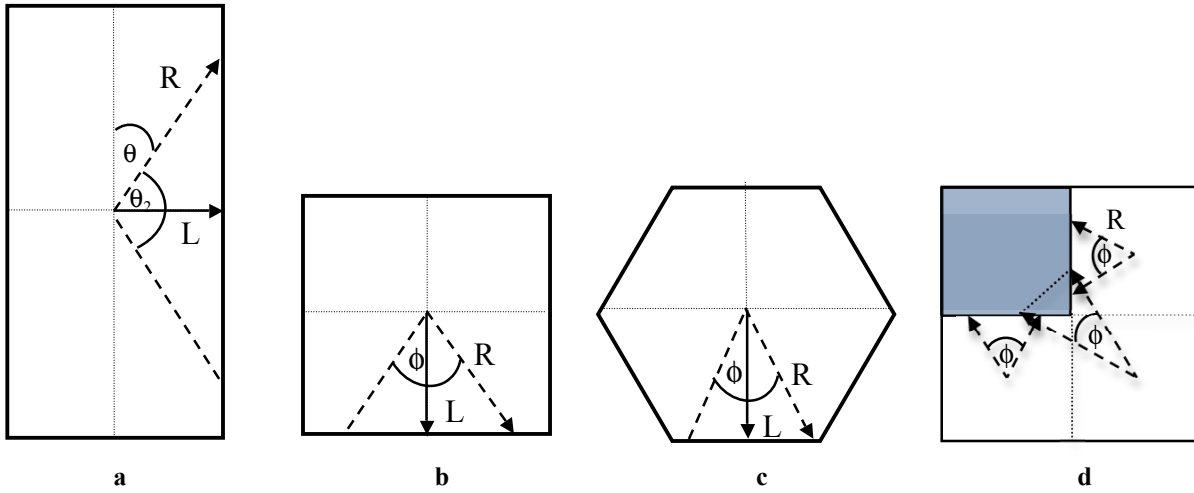

Figure 2: Calculated solid angle components: Polar angle θ for all designs (a) and azimuthal angle φ for square hole (b), pillar (b), hexagonal hole (c), and pillar (d) configurations

The polar angle is calculated in the same way for all geometries (fig.2a), with the integration bounds for θ given by

$$\theta_{1,2} = \frac{\pi}{2} \pm \cos^{-1}\left(\frac{L}{2R}\right) \tag{7}$$

where L is replaced by w_t for the parallel trench, l_s for the square hole and pillar, and l_h for the hexagonal geometry. The azimuthal angle is calculated similarly for all designs except the pillar configuration by

$$\phi = \sum_{i=1}^{n} \int_{0}^{\cos^{-1}\left(\frac{L}{2R}\right)} d\phi \tag{8}$$

where n is the number of walls in each structure and L is replaced by w_t, l_s, or l_h for the trench, square hole, or hexagonal geometry, respectively. If the range R exceeds the maximum distance to any wall, the azimuthal angle is simply integrated over 2π.

The pillar design is slightly more complicated; in the unit cell shown in figure 2d, it is apparent that there are three possible interaction quadrants. Assuming particle emission and distribution are the same as previously stated, the average interaction sites are located in the center of each quadrant. The azimuthal angle for each quadrant can be calculated by

$$\phi_{1,2} = 2 \cdot \begin{cases} 0 & ; R \le \frac{s_s}{2} \\ \cos^{-1}\left(\frac{s_s}{2R}\right) & ; R \ge \frac{s_s}{2} \text{ and } \frac{l_s}{2} < \sqrt{R^2 + s_s^2} \\ \sin^{-1}\left(\frac{l_s}{2R}\right) & ; \text{else} \end{cases} \qquad \phi_3 = 2 \cdot \begin{cases} 0 & ; R \le \frac{\sqrt{2} \cdot s_s}{2} \\ \left[\frac{\pi}{4} - \sin^{-1}\left(\frac{s_s}{2R}\right)\right] & ; R \ge \frac{\sqrt{2} \cdot s_s}{2} \\ \sin^{-1}\left(\frac{\sqrt{2} \cdot l_s}{2R}\right) & ; \phi \ge \sin^{-1}\left(\frac{\sqrt{2} \cdot l_s}{2R}\right) \end{cases} \tag{9}$$

where s_s is the spacing between pillars and l_s is the width of the pillar. These limits take into account the following: no particle will reach a pillar if the distance to a pillar exceeds the range, only two pillars can be reached by the reaction particles in each quadrant, and the acceptance angle for each pillar is limited by the pillar width. The total solid angle ϕ_t can now be calculated using

$$\phi_t = \phi_1\left(\frac{s_s \cdot l_s}{2(s_s \cdot l_s) + s_s^2}\right) + \phi_2\left(\frac{s_s \cdot l_s}{2(s_s \cdot l_s) + s_s^2}\right) + \phi_3\left(\frac{s_s^2}{2(s_s \cdot l_s) + s_s^2}\right) \tag{10}$$

where the fractional angle ϕ for each quadrant is weighted by the combined area of all three quadrants.

Total device efficiency for can now be calculated by

$$E_g = \left(1 - e^{-\Sigma_a x_D}\right)\left(F_g\right)\left(\frac{\Omega_g}{4\pi}\right) \tag{11}$$

where g denotes the particular device geometry. By inspection of equations 1-10, it can be seen that the device efficiency, for a given converter, is dependent only on the depth of the converter, the width of the converter structure, and the spacing between them. Calculation of initial parameter values for the simulations was done by setting incident neutron energy to 0.0235 eV, fixing the converter depth (x_D) at 40 μm, and varying the converter thickness.

2009 International Conference on Mathematics, Computational
Methods & Reactor Physics (M&C 2009), Saratoga Springs, NY, 2009

5/12

The calculations assume that upon reaching the silicon, all the remaining charged particle energy is deposited. This is not realistic at small separation values; for a sufficiently thin silicon wall, charged particles can penetrate into adjacent converter structures without depositing enough energy to meet the LLD. As a result, the calculations revealed no optimal silicon thickness for any of the configurations, with maximum device efficiency occurring at a minimum separation value of 0.25 µm. The highest efficiency, 73%, was calculated for the hexagonal design using an optimal hole radius of 3.2 µm. A hole width of 2.5 µm resulted in an efficiency of 70% for the square design, and a maximum efficiency of 64% was found with a separation distance of 1.5 µm for the pillar design. The parallel trench design, with an optimal trench width of 1.75 µm, exhibited the lowest efficiency of all the configurations at 60%.

2.2. Monte Carlo Simulations

Two software packages were considered for the detector simulations: The GEANT4 Monte Carlo toolkit [10] and MCNPX [11]. MCNPX, while considered to be the de facto standard for neutron transport, has a major disadvantage for this application: an inability to produce and track the ^{10}B reaction products. The GEANT4 toolkit, in contrast, is capable of producing and tracking virtually all subatomic particles, charged or neutral. Developed largely at the European Organization for Nuclear Research (CERN), the toolkit is collection of C++ class libraries, freely available under an open license. Although more difficult to implement than MCNP5, considering that the user must write their own simulation, GEANT4 has a flexibility of simulation design that is unparalleled. For these reasons, GEANT4 was chosen over MCNPX for this work.

2.1.1. Simulation Physics

In GEANT4 the neutron physics processes are split into 2 groups; low energy, where 0.025 eV < E < 20 MeV, and high energy, where E > 20MeV. The low energy processes, utilized here, have tabulated cross-sections taken from the ENDF/B-VII libraries, consisting of elastic scattering, inelastic scattering, radiative capture, and fission. The standard electromagnetic (EM) library, valid down to approximately 500eV, was utilized for photon and charged particle transport. For use in this work, several processes were removed from the EM package to decrease simulation time: bremsstrahlung and pair production were removed due to low probability, scintillation was removed for lack of relevance, and muon production/transport was eliminated.

Each physics process that produces secondary particles can have a production threshold applied, below which no particles are created. The production threshold is set in units of distance, corresponding to particle range, by the user and converted to energy by the software. If an interaction creates a secondary particle below this threshold, the energy that would have been imparted to the secondary is deposited directly at the interaction site. These threshold limits are used to decrease the number of particles that are tracked, reducing the simulation time, but consequently lowering simulation accuracy. Thresholds were set at 500 nm for photons and electrons in all simulations. Given that most of the structures in each detector are larger than 1µm, the simulation speed was increased with negligible effect on accuracy.

2.1.2. Simulation Geometry

The geometrical components of the simulation are composed of three parts: the materials used for each component, its associated physical geometry, and the geometric configuration of the neutron source.

GEANT4 allows for users to specify the elements, isotopes, and materials used in each simulation. These can either be created from scratch by the user or taken from the GEANT4 database, which is derived from the National Institute of Standards and Technology's (NIST) database of elements and isotope compositions. The following materials were used for all the simulations:

- Air- Taken from the database, this is the default material for the simulation world. It is composed of 78% nitrogen and 22% oxygen, and has a density of 1.290 mg/cm^3.
- Monocrystal Silicon- Also taken from the database, this is the base material for the detector, composed of pure silicon and having a density of 2.3290 g/cm^3.
- Enriched Boron- Composed of 99% ^{10}B and 1% ^{11}B, each isotope was explicitly defined (protons, neutrons, atomic mass) and combined in the correct ratio. Density was set to 2.14 g/cm^3, reflecting the lower atomic mass of ^{10}B.

The simulated geometries for all designs were similar, consisting of a 5cm x 5cm x 60µm silicon base, etched 40 µm deep with the correct structures and filled with enriched boron. The starting parameters for the etched structures were determined by the previous analytical calculations, then varied over the same range. These parameters were: trench and wall widths for trench design (fig.1a), length of side and separation for the square holes (fig.1b), and length of a side and separation for the pillar design (fig.1b), and minor radius and separation for the hexagonal holes (fig.1c).

The analytical calculations assume that neutrons are incident normal to the surface, as well as distributed evenly over the entire detector. To achieve this in the simulations, the source was modeled as a square plane, 5 mm square, positioned 2 cm above the detector surface. Neutron emission distribution is even across the entire source and directed at the detector, such that every neutron emitted by the source strikes the detector. To ensure adequate statistics, 10^7 neutrons were simulated for each run. Figure 3 below shows the details of a simulated detector. A total of 60 simulations were run per device configuration.
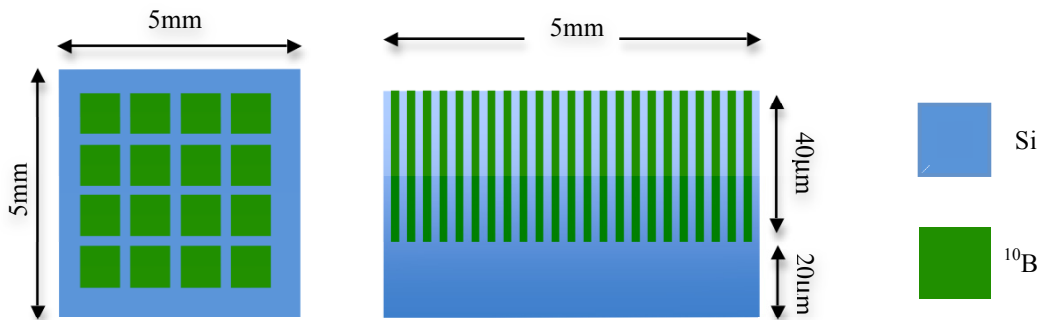

Figure 3: Simulated Detector Detail

2009 International Conference on Mathematics, Computational
Methods & Reactor Physics (M&C 2009), Saratoga Springs, NY, 2009

7/12

Simulation of the parallel trench design (fig.4) revealed an optimal efficiency of 43 percent, occurring at a trench width of 1.5 µm and a corresponding silicon thickness of 0.75 µm. Although the highest efficiency achieved, 45 percent, indicates optimums of 0.75 µm and 0.25 µm for trench and wall widths, the sub-micron levels at which this occurs is beyond current university manufacturing capabilities, and as such is not considered.
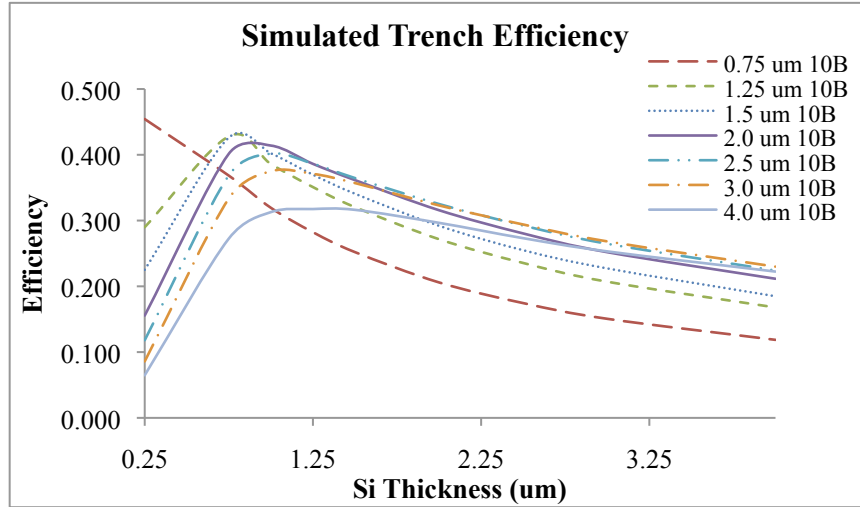

Figure 4: Parallel Trench design simulated efficiency

A comparison of the analytical and simulated results at the 1.5 µm optimal trench width reveals excellent agreement at silicon thicknesses greater than 0.75 µm (fig.5). The deviation of the two methods below this value can be attributed to the previously discussed limitation of the analytic calculations.

2009 International Conference on Mathematics, Computational
Methods & Reactor Physics (M&C 2009), Saratoga Springs, NY, 2009
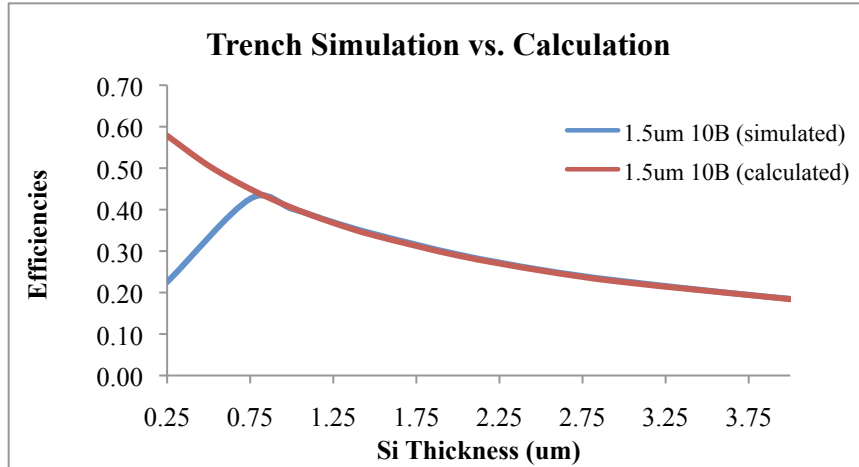
8/12

Trench Simulation vs. Calculation

Figure 5: Comparison of simulated and calculated results for parallel trench design

Simulation of the square hole design showed an optimal hole width of 2 µm and a hole separation of 0.5 µm, resulting in an efficiency of 47 percent. It can be seen in figure 6 that, for hole widths of 1.5 µm to 2.5 µm, maximum efficiency is nearly identical.
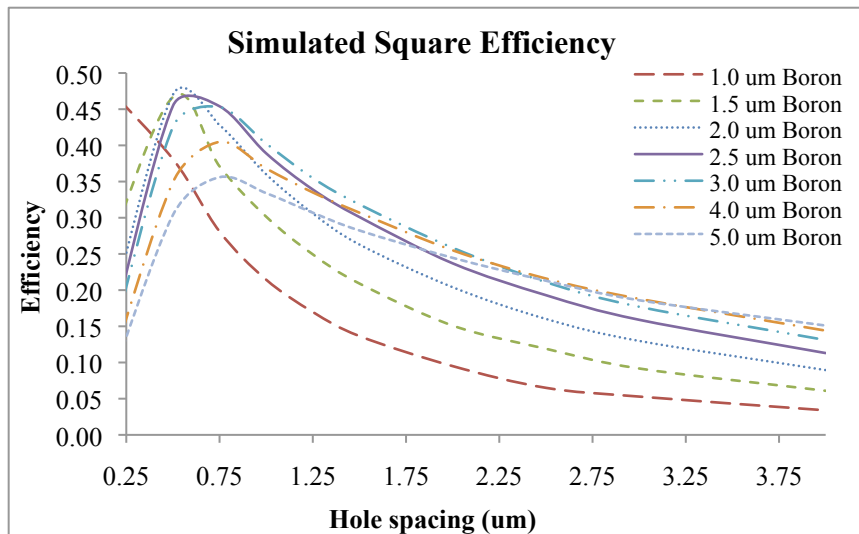
Simulated Square Efficiency

Figure 6: Square hole design simulated efficiency

The simulated hexagonal design (fig.6) showed a higher efficiency than the square, but it was only a slight increase, from 47 to 48 percent. It can be seen in figure 7 that for hex radii from 2 to 3 µm, efficiencies are almost identical, similar to the square hole design. The parameter values

2009 International Conference on Mathematics, Computational
Methods & Reactor Physics (M&C 2009), Saratoga Springs, NY, 2009

9/12

corresponding to maximum efficiency were a minor hex diameter of 2.8μm and a hole separation of 1μm.
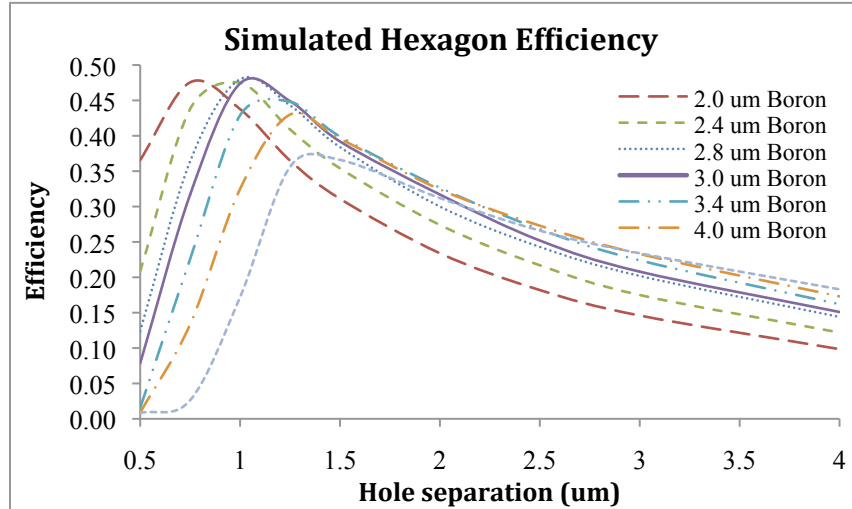

Figure 6: Hexagonal hole design simulated efficiency

Results from the simulation of the pillar geometry (fig.7) revealed a maximum efficiency of 40 percent, achieved with a pillar width of 1.25 μm and 1.0 μm pillar spacing. This design showed greatest variation in efficiency, with a maximum difference of ~12 percent from 1μm to 1.5μm pillar spacing.
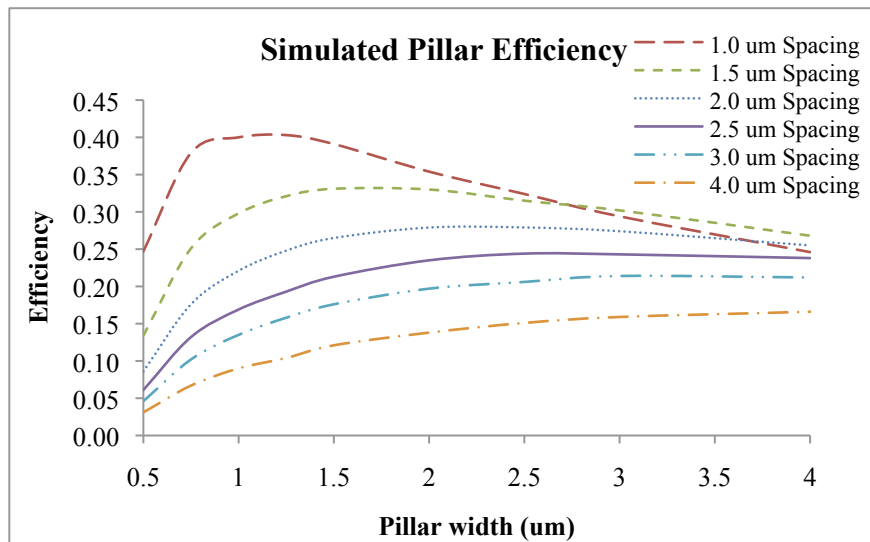

Figure 7: Pillar design simulated efficiency

3. CONCLUSIONS

The ability to create extremely small (< 2μm) structures in a detector, when combined with the charge collection advantage afforded by continuous p-n junctions, allows for a solid-state detector with very high theoretical thermal neutron detection. All designs under consideration consisted of a silicon base with structures etched into it and backfilled with a thermal neutron converter. By performing first-order analytical calculations, each design's initial optimization parameters were determined. Monte Carlo simulations of the designs under consideration revealed ideal device parameter values and resulted in a maximum theoretical efficiency of 48 percent for the hexagonal hole design, followed closely by the square hole design at 47 percent. The parallel trench design showed a maximum realistic efficiency of 43 percent, a slight increase over the pillar configuration at 40 percent. Additionally, the two etched hole designs demonstrated efficiency variances of 1 percent or less over a 1μm range of hole sizes. This would seem to indicate a greater manufacturing tolerance, making the etched hole designs the most preferable of those presented in this work. Future work will include the simulation of non-ideal source geometry, detector response to a polyenergetic neutron source (i.e. Watt spectrum), and efficiencies of multiple detector configurations.

2009 International Conference on Mathematics, Computational
Methods & Reactor Physics (M&C 2009), Saratoga Springs, NY, 2009

11/12

REFERENCES

1. A Rose, "Sputtered boron films on silicon surface barrier detectors", *Nuclear Instrumentation and Methods*, **52**, pp.166–70, (1967).
2. F Shiraishi, Y Takami, H Husimi, S Ohkawa, C Kim, Y Kim, K Kikuchi, and T Sakai, "A new fast neutron spectrometer made of epitaxial integrated de-e Si Detector", *Nuclear Science, IEEE Transactions on*, **32(1)**, pp.471 – 475, (1985).
3. F Shiraishi, Y Takami, T Hashimoto, and K Hatori, "A new type personnel neutron dosimeter with thin Si detectors", *Nuclear Science, IEEE Transactions on*, **35(1, Part 1-2)**, pp.575 – 578, (1988).
4. A Mireshghi, G Cho, J Drewery, T Jing, S Kaplan, V Perez-Mendez, and D Wildermuth, "Amorphous silicon position sensitive neutron detector", *Nuclear Science, IEEE Transactions on*, **39(4)**, pp.635 – 640, (1992).
5. Petrillo, C., Sacchetti, F., Toker, O., & Rhodes, N. (1996, Jan 1). "Solid state neutron detectors", *Nuclear Instruments and Methods in Physics Research A,* **378**, pp.541-551*,* (1996).
6. D Mcgregor, M Hammig, Y Yang, & H Gersch, "Design considerations for thin film coated semiconductor thermal neutron detectors—I: basics regarding alpha particle emitting neutron reactive films", *Nuclear Instruments and Methods in Physics Research A ,* **500 (1-3)**, pp.272-308, (2002).
7. J Shultis & D Mcgregor, "Efficiencies of coated and perforated semiconductor neutron detectors", *IEEE Nuclear Science Symposium Conference Record,* **7**, pp.4569 – 4574, (2004).
8. N LiCausi, J Dingley, Y Danon, J Lu, and I B Bhat, "A novel solid state self-powered neutron detector", *Proc. SPIE,* **7079***,* (2008)
9. G. F. Knoll, *Radiation Detection and Measurement 3rd Ed*, Wiley and Sons, City & Country (1999).
10. S. Agostinell et al, "GEANT4—A Simulation Toolkit," *Nuclear Instruments and Methods in Physics Research Section A*, **506**, pp. 250-303, (2003).
11. G. W. McKinney et al., "*MCNPX Overview*", Proceedings of the 2006 HSSW, FNAL, IL, September 6-8, 2006.

2009 International Conference on Mathematics, Computational Methods & Reactor Physics (M&C 2009), Saratoga Springs, NY, 2009

12/12